Journal of The Electrochemical Society, **146** (10) 3582-3590 (1999)
S0013-4651(99)01-045-9 CCC: $7.00 © The Electrochemical Society, Inc.

Reaction Kinetics and X-Ray Absorption Spectroscopy Studies of Yttrium-Containing Metal Hydride Electrodes

E. A. Ticianelli,* S. Mukerjee,* J. McBreen,* G. D. Adzic,* J. R. Johnson,* and J. J. Reilly*

Department of Applied Science, Brookhaven National Laboratory, Upton, New York 11973, USA

This is a study of electrode degradation mechanisms and reaction kinetics of $LaNi_{4.7}Sn_{0.3}$, $La_{(1-x)}Y_xNi_{4.7}Sn_{0.3}$ (x = 0.1, 0.2, and 0.3) and $La_{0.7}Y_{0.3}Ni_{4.6}Sn_{0.3}Co_{0.1}$ metal hydride electrodes. Alloy characterization included X-ray diffraction, X-ray absorption (XAS), hydrogen absorption in a Sieverts apparatus, and electrochemical cycling of alloy electrodes. The atomic volume of H was determined for two of the alloys. Electrochemical kinetic measurements were made using steady-state galvanostatic measurements, galvanodynamic sweep, and electrochemical impedance techniques. XAS was used to examine the degree of corrosion of the alloys with cycling. Alloying with Y decreased the corrosion rate. The results are consistent with corrosion inhibition by a Y-containing passive film. The increase in the exchange current density of the hydrogen oxidation reaction with increasing depth of discharge was much greater on the Y-containing alloys. This may be due to the dehydriding of the catalytic species on the surface of the metal hydride particles.
© 1999 The Electrochemical Society. S0013-4651(99)01-045-9. All rights reserved.

Manuscript submitted January 12, 1999; revised manuscript received May 28, 1999.

Previous studies have shown that $LaNi_5$ alloy modifications affect the cycle life and hydrogen absorption capacity of AB_5 metal hydride (MH) electrodes, but sometimes the reasons for these effects are not well understood.[1-6] The effects of various ternary substitutions of Ni in $LaNi_5$ have been studied, and the results show that cycle life improves with ternary substituents in the order Mn < Ni < Cu < Cr < Al < Co. [1] The effect of Co substitution has been attributed to a diminution in the volume changes upon hydrogen absorption and desorption and to a surface passivation mechanism (*i.e.*, oxide formation).[2] Ratnakumar *et al.*[1,3-6] described the advantage associated with using Sn as a ternary substituent, as compared to In, Ge, Si, and Al. The addition of small amounts of Sn improves cycle life and the kinetics of hydrogen absorption and desorption with a slight reduction in specific capacity.

In commercial AB_5 electrodes, pure La is substituted by mischmetal (Mm), a naturally occurring mixture of the rare earth metals, corresponding mainly to (in atom percent, atom %): 50-55 Ce, 18-28 La, 12-18 Nd, and 4-6 Pr. [7] A typical composition for use in batteries is $MmNi_{3.5}Co_{0.75}Mn_{0.4}Al_{0.3}$. [8] Apart from La, Ce is the predominant rare earth in normal Mm, and thus the role of Ce has been investigated in some detail.[7,9] Results indicate an improvement in the cycle life due to the presence of Ce, and this effect has been attributed to the formation of a passivating Ce oxide.[9,10]

Our recent studies show that X-ray absorption spectroscopy (XAS) is a very useful technique for the study of alloy hydrides and particularly the role of the electronic structure, the environment around minor constituents, and the corrosion of individual components in the alloy.[7,9-11]

The effect of La or Ni substituents on the kinetics of the hydrogen oxidation reaction (HOR) and the absorption process has not been investigated in a systematic way. Most kinetic studies have used transient and steady-state polarization techniques,[12-19] and electrochemical impedance spectroscopy (EIS).[20-28] Previous studies have reported on the influence of several electrode parameters on the reaction kinetics of the HOR. These include the influence of electrode structure and the nature of the support of the metal hydride alloy powder. Attempts have been made to characterize the electrode reaction mechanism, the role of diffusion processes, and the effects of alloy particle geometry on the polarization response. It is clear from this work that the electrode processes are very complex and that the kinetics of the hydriding/dehydriding reactions is not yet completely elucidated.

This work is a study of the effect of Y as a substituent for La on the cycle life and charge/discharge reaction kinetics. The alloys included $LaNi_{4.7}Sn_{0.3}$, $La_{(1-x)}Y_xNi_{4.7}Sn_{0.3}$ (x = 0.1, 0.2, and 0.3), and $La_{0.7}Y_{0.3}Ni_{4.6}Sn_{0.3}Co_{0.1}$. Studies included measurements of charge/discharge characteristics, cycle life studies, galvanodynamic potential *vs*. current profiles, and electrochemical impedance spectra at several states of charge and at several temperatures. XAS was used to characterize the corrosion products in cycled electrodes.

Experimental

Alloy preparation and characterization.—All the alloys were prepared from high purity (>99.9%) starting materials by an arc-melting technique followed by an annealing step at a temperature of 1173 K for 48 h. X-ray diffraction (XRD) patterns were obtained for each alloy, and their lattice parameters determined. The molar volume of hydrogen in the hydride phase was also determined. Details of these procedures are given elsewhere.[7]

Cycling and electrochemical studies.—The alloys were first activated by subjecting each to several hydriding/dehydriding cycles in a Sieverts apparatus. This produced a fine powder with a typical Brunauer-Emmett-Teller (BET) surface area of *ca*. 0.5 m^2/g, or a particle size of *ca*. 5 μm. Electrodes were prepared by pressing a mix comprised of 0.1 g of the alloy powder, 0.1 g carbon black (Monarch 2000), and 33 weight percent (wt %) polytetrafluoroethylene (PTFE) binder (Teflon T30), on both sides of an 80 mesh nickel screen disk with a geometric area of 2.0 cm^2. This electrode structure gives reproducible results and is durable with cycling. In tests with over 600 electrodes at our laboratory, it has been shown that in all cases cycle life was limited by the alloy materials and not by degradation of the electrode structure. Electrochemical measurements were done in a three-electrode cell in 6 M KOH, with a Pt mesh counter electrode and a Hg/HgO reference electrode.

Life-cycle tests were done by charging at *ca*. a C/3 rate (10 mA) for 4 h and discharging at the same rate to a cutoff cell potential of 0.7 V *vs*. Hg/HgO. Tests on six samples showed that the capacity *vs*. cycle life data were reproducible to within ±5%. The electrochemical impedance spectra were obtained in the frequency range of 10 kHz to 1 mHz, with an ac amplitude of 5 mV, with the electrodes maintained at the open-circuit potential. Galvanodynamic potential *vs*. current profiles (GYP) were obtained for the electrodes at several states of charge (SOC) with the cell thermostated at 10, 25, 40, and 55°C, using a Solartron potentiostat. GYP profiles were recorded at a scan rate of 0.01 mA s^{-1} for currents varying within ±1.5 mA.

X-ray absorption spectroscopy.—XAS measurements were made on both uncycled and cycled alloy powders. After cycling the electrode material was removed from the current collector, washed with

* Electrochemical Society Active Member.

Downloaded on 2017-02-26 to IP 129.10.247.223 address. Redistribution subject to ECS terms of use (see ecsdl.org/site/terms_use) unless CC License in place (see abstract).

S0013-4651(99)01-045-9 CCC: $7.00 © The Electrochemical Society, Inc.

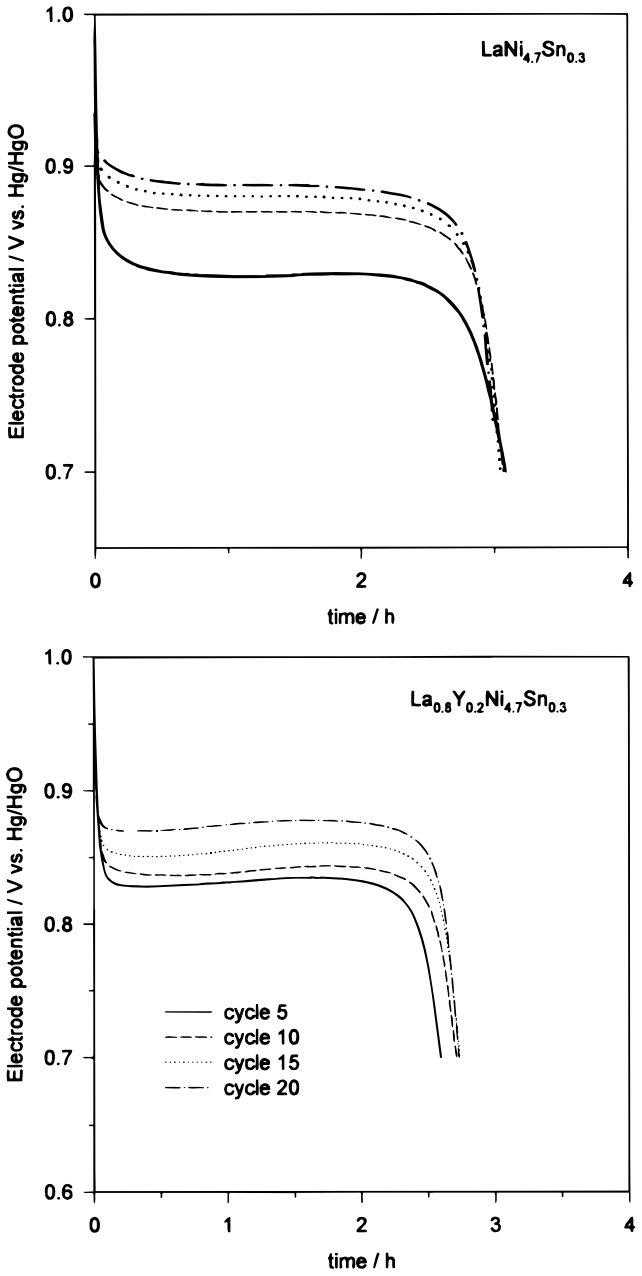

Figure 1. Discharge profiles for the LaB_5 and $La_{0.8}Y_{0.2}B_5$ alloys (B_5 = $Ni_{4.7}Sn_{0.3}$) after 1, 5, 10, 15, and 20 charge/discharge cycles. Discharge current = 100 mA g^{-1} (C/3).

deionized water to remove KOH, and ultrasonically dispersed in acetone. After drying, the disk pellet for XAS analysis was prepared by pressing these materials on the top of a PTFE-bonded porous carbon substrate (E-TEK).

The XAS at the Ni K edge were done in both the transmission and electron yield modes. In the transmission mode, results are more sensitive to properties of Ni atoms in bulk alloy. According to a previous calculation,[10] using a method described in the literature,[29] at the energy of the Ni K edge, the electron-yield measurements provide surface sensitive XAS of the alloy particles to a depth of *ca*. 200 to 250 Å. XAS at the Y K edge were done in the transmission mode. The XAS data analysis was done according to procedures described in detail elsewhere.[30-32]

Results and Discussion

Electrode capacity, steady-state kinetics, and capacity decay.—Figure 1 shows typical discharge profiles obtained for the LaB_5 and $La_{0.8}Y_{0.2}B_5$ alloys (B_5 = $Ni_{4.7}Sn_{0.3}$) after 1, 5, 10, 15, and 20 charge/discharge cycles. Table I shows the values of the maximum discharge capacity obtained for each alloy, together with the capacity decay rates with cycling. Also included, for two alloys (LaB_5 and $La_{0.8}Y_{0.2}B_5$), are the atomic volumes of H in the hydride phase, the number of H atoms per unit cell, and the expansion of the unit cell due to charging. Plots of the discharge capacity normalized with respect to the maximum capacity are presented in Fig. 2 for the alloys containing 0, 0.1, and 0.2 atomic fraction (x) of Y with respect to the total amount of Y and La.

Results in Fig.1 and 2 show that in the initial cycles the capacity first increases with cycle number, reaches a maximum, and thereafter decreases with cycling due to corrosion of the alloy. The number of cycles required for alloy activation was dependent on the composition, and increased with higher yttrium content.

The sample with $x = 0.2$ exhibited the highest stability (*i.e.*, lowest rate of capacity loss) whereas the alloy with $x = 0$ (no Y) had the largest capacity decay (Table I). There was no apparent direct correlation between the capacity decay and the volume changes occurring in the alloys during cycling. The maximum value of discharge capacity decreases with increasing Y content in the alloy. Increasing Y content decreases the unit cell volume and increases the hydrogen plateau pressure. The plateau pressure becomes unacceptably high at ambient temperature when $x > 0.3$. This sets an upper limit on the Y content. The data in Fig. 2 and Table I show that after 100 cycles the alloys with $x = 0.2$ and with $x = 0$ have the same capacity (240 mAh g^{-1}). With further cycling the former shows superior performance. At 300 cycles, the respective capacity for $LaNi_{4.7}Sn_{0.3}$ and $La_{0.8}Y_{0.2}Ni_{4.7}Sn_{0.3}$ was 100 and 200 mAh g^{-1}, indicating a considerable improvement of cycling stability promoted by Y.

The results in Fig. 1 show an increase in the electrode discharge potential during the activation process. In the sample with Y, there was a clear increase in electrode potential with increasing depth of discharge. This indicates that the overall kinetics of the HOR changes with the depth of discharge, with Y playing an important role.

Galvanodynamic and EIS studies.—Figure 3 presents examples of the gavanodynamic discharging profiles obtained at 25°C with the electrodes at a 100% state of charge. To avoid polarization effects related to hydrogen atom transport processes in the galvanodynamic

Table I. Alloy characteristics and capacity decay on cycling; Q_{max} is the maximum capacity.

Alloy	Q_{max} (mAh g^{-1})	V_H [a] ($Å^3$)	H atoms/unit cell	Volume expansion[b] (%)	Decay (%/cycle)
$LaNi_{4.7}Sn_{0.3}$	308	3.26	5.05	18.4	0.22
$La_{0.9}Y_{0.1}Ni_{4.7}Sn_{0.3}$	287	—	4.71	—	0.16
$La_{0.8}Y_{0.2}Ni_{4.7}Sn_{0.3}$	268	3.11	4.36	15.4	0.10
$La_{0.7}Y_{0.3}Ni_{4.7}Sn_{0.3}$	198	—	—	—	~0.16
$La_{0.7}Y_{0.3}Ni_{4.6}Sn_{0.3}Co_{0.1}$	221	—	—	—	~0.10

[a] Atomic volume of H in the hydride phase.
[b] Expansion of unit cell in charge cycle.

Downloaded on 2017-02-26 to IP 129.10.247.223 address. Redistribution subject to ECS terms of use (see ecsdl.org/site/terms_use) unless CC License in place (see abstract).

S0013-4651(99)01-045-9 CCC: $7.00 © The Electrochemical Society, Inc.

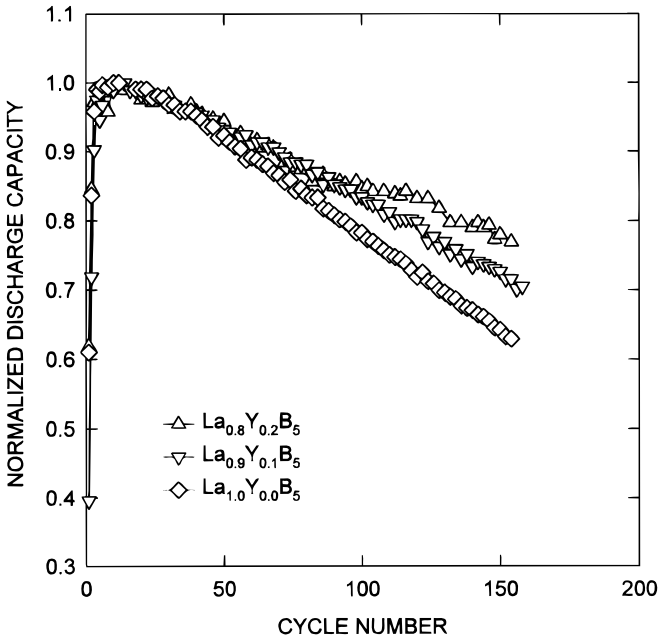

Figure 2. Normalized discharge capacity *vs.* cycle number for three $La_{(1-x)}Y_xNi_{4.7}Sn_{0.3}$ electrodes (x = 0, 0.1, and 0.2). Charge/discharge currents C/3; charging time 4 h; discharge cuttoff potential −0.7 V *vs.* Hg/HgO.

method, the reaction kinetics was studied in a very-low-current-density range. For these conditions the polarization of the electrode can be treated assuming that the charge-transfer step in the charge/discharge mechanism (where S is an active site at the alloy surface) is the rate-determining step.[28] The overall mechanism is

$$H_2O + S + e^- \rightleftarrows S\text{–}H_{ads} + OH^- \quad \text{(charge transfer)} \quad [1]$$

$$S\text{–}H_{ads} \rightleftarrows S\text{–}H_{abs(surface)} \quad \text{(adsorption)} \quad [2]$$

$$S\text{–}H_{abs(surface)} \rightleftarrows S\text{–}H_{abs(bulk)} \quad \text{(diffusion)} \quad [3]$$

$$S\text{–}H_{abs(bulk)} \rightleftarrows S\text{–}H_{abs(bulk)} \quad \text{(phase transition)} \quad [4]$$

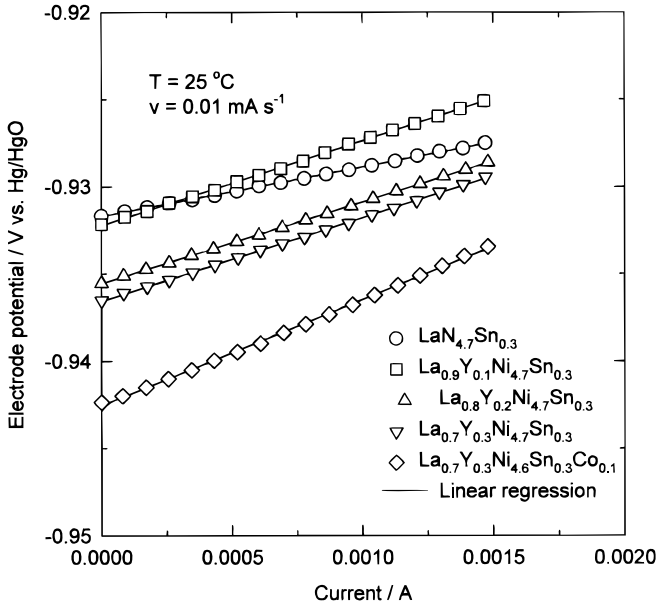

Figure 3. Galvanodynamic profiles (E *vs.* j) at 25°C for $LaNi_{4.7}Sn_{0.3}$, $La_{(1-x)}Y_xNi_{4.7}Sn_{0.3}$ (x = 0.1, 0.2, and 0.3), and $La_{0.7}Y_{0.3}Ni_{4.6}Sn_{0.3}Co_{0.1}$ electrodes. Scan rate 0.01 mA s^{-1}.

Also, for these conditions the catalytic activity can be measured by the value of the exchange current density (j_o), which can be obtained from the slope of the polarization curves (j *vs.* η) at low reaction overpotential (η) using the equation

$$j_o = \frac{RT}{F}\left(\frac{j}{\eta}\right)_{\eta\to 0} \quad [5]$$

where F is Faraday's constant, R is the gas constant, and T is the temperature. Values of j_o were obtained for activated and cycled metal hydride alloys at 100% state of charge (SOC), and some representative results are summarized in Table II. The activation energy, obtained from Arrhenius plots (log j_o *vs.* 1/T), are also presented in Table II.

Figures 4 and 5 show impedance plots of activated $LaNi_{4.7}Sn_{0.3}$ and $La_{0.8}Y_{0.2}Ni_{4.7}Sn_{0.3}$ alloy electrodes (four cycles and 20 cycles, respectively) in the form of Nyquist or Cole-Cole plots at several SOCs at 25 and 40°C. In Fig. 6, data at 10 and 25°C were plotted with an expanded scale for the region of high frequency for the activated $La_{0.8}Y_{0.2}Ni_{4.7}Sn_{0.3}$ alloy electrode to highlight the impedance features in this region. Figure 7 presents the results obtained at several temperatures for the activated and fully charged $La_{0.8}Y_{0.2}Ni_{4.7}Sn_{0.3}$ hydride electrode.

For both electrodes at the several SOCs and temperatures, it is observed that in the high-frequency range that the impedance spectra show an arc coupled to an apparent linear region. In the lower-frequency region, another arc is seen which depends on the temperature and the state of charge and is coupled to another feature related to a moderate or a steep increase of the imaginary component of the impedance. It should be noted that these impedance responses are similar to results presented for many other metal hydride alloys.[20-28] Interpretation of these features has been a matter of con-

Table II. Electrode kinetic parameters, exchange current j_0, and activation energy obtained from galvanodynamic measurements.

Hydrogen oxidation reaction-SOC 100%

Alloy	j_o at 25°C (mA g^{-1})	Activation energy (kJ mol^{-1})
$LaNi_{4.7}Sn_{0.3}$		
- activated (eight cycles)	88	34
- 130 cycles	194	
$La_{0.9}Y_{0.1}Ni_{4.7}Sn_{0.3}$		
- activated (20 cycles)	53	35
$La_{0.8}Y_{0.2}Ni_{4.7}Sn_{0.3}$		
- activated (20 cycles)	52	35
- 130 cycles	148	
$La_{0.7}Y_{0.3}Ni_{4.7}Sn_{0.3}$		
- activated (20 cycles)	52	30
$La_{0.7}Y_{0.3}Ni_{4.6}Sn_{0.3}Co_{0.1}$		
- activated (22 cycles)	41	32

Hydrogen evolution reaction

Alloy	j_o at 25°C (mA g^{-1})	Activation energy (kJ mol^{-1})
$LaNi_{4.7}Sn_{0.3}$		
- activated (eight cycles)	103	34
- 130 cycles	227	
$La_{0.9}Y_{0.1}Ni_{4.7}Sn_{0.3}$		
- activated (20 cycles)	55	40
$La_{0.8}Y_{0.2}Ni_{4.7}Sn_{0.3}$		
- activated (20 cycles)	58	43
- 130 cycles	164	
$La_{0.7}Y_{0.3}Ni_{4.7}Sn_{0.3}$		
- activated (20 cycles)	54	40
$La_{0.7}Y_{0.3}Ni_{4.6}Sn_{0.3}Co_{0.1}$		
- activated (22 cycles)	43	38

Downloaded on 2017-02-26 to IP 129.10.247.223 address. Redistribution subject to ECS terms of use (see ecsdl.org/site/terms_use) unless CC License in place (see abstract).

S0013-4651(99)01-045-9 CCC: $7.00 © The Electrochemical Society, Inc.

troversy. Zhang *et al.*[21] assigned the arc in the higher-frequency region (from 20 kHz to 520 Hz) to the impedance between the current collector and the active material. They attributed the features at the middle-frequency range (from 130 to 12 Hz) to the particle-to-particle electronic conductance of the MH electrodes, and the arc at low frequency (from 10 Hz to 10 mHz) to the charge-transfer step at the electrode/electrolyte interface. However, more recently, based on ac modeling of the kinetics of metal hydride electrodes, Wang[28] attributed these three features, seen at decreasing frequencies, to the charge-transfer reaction, surface absorption, and hydrogen diffusion, as represented by reactions 1, 2, and 3 above. Based on previous work[20-28] and the present results, the following assignments are proposed for the observed impedance features.

1. Arc in the range of 8 kHz to 200 Hz.—Figures 6 and 7b show that the magnitude of the high-frequency arc varies only slightly with temperature and cannot be assigned to either the charge-transfer step[28] or to the diffusion of hydrogen. The results are consistent with a contact resistance between the current collector and the active material, as originally proposed by Zhang *et al.*[21] The increase in the magnitude of the arc with decrease of the SOC (inset of Fig. 6) can be explained by an increase in the contact resistance resulting from the volume contraction of the MH particles occurring upon alloy discharge (Table I). The small temperature dependence of this arc, which is more pronounced at low SOC, may also be related to the volume change of the particles.

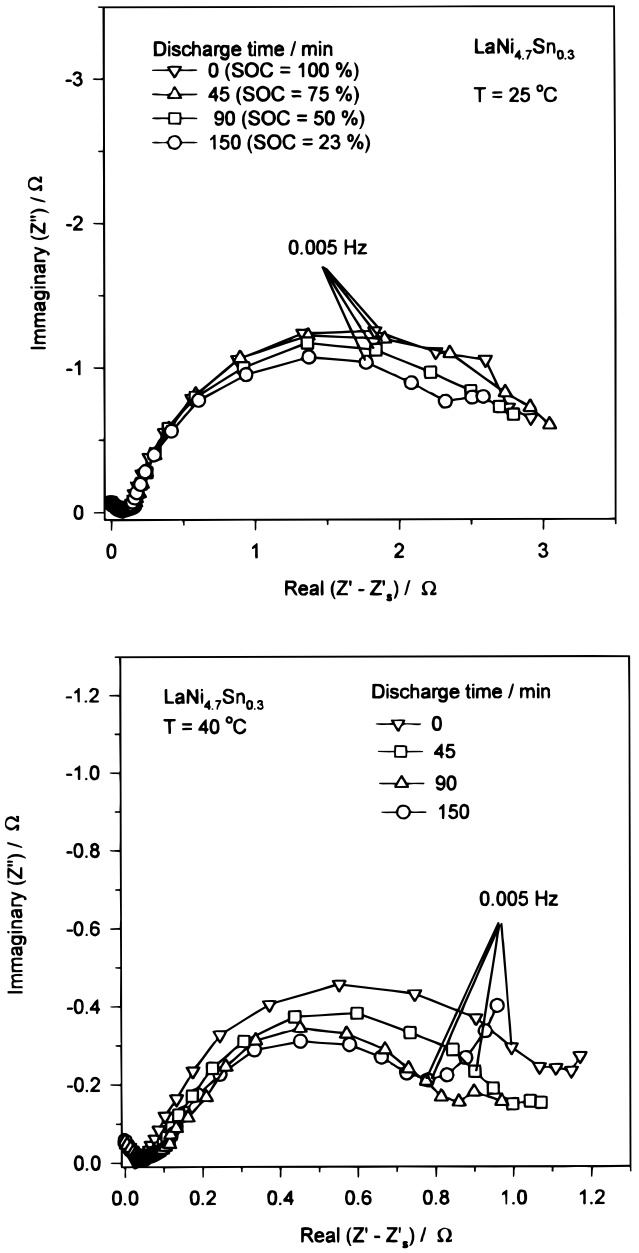

Figure 4. Nyquist plots at several states of charge (SOC) for a $LaNi_{4.7}Sn_{0.3}$ electrode at 25 and 40°C. Frequency range: 10 kHz to 0.001 Hz. Real part was corrected for the ohmic resistance between the working and the reference electrode. Measurements were made at open-circuit potential.

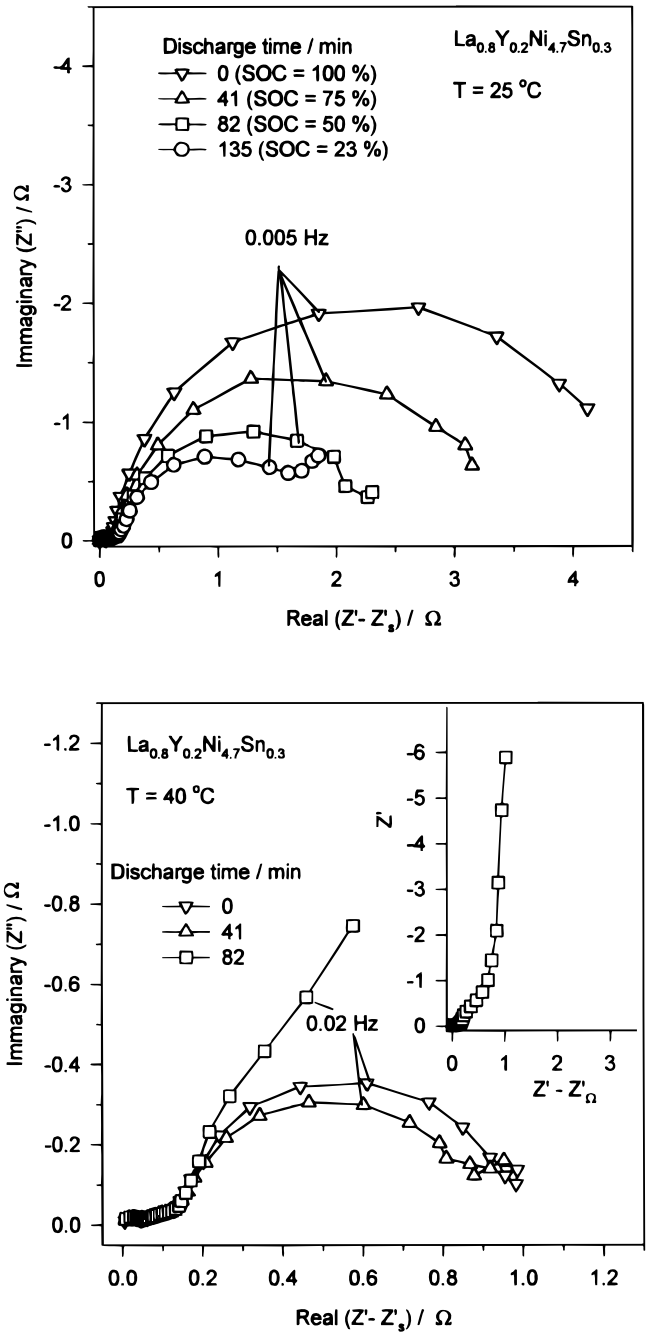

Figure 5. Nyquist plots at several SOC for a $La_{0.8}Y_{0.2}Ni_{4.7}Sn_{0.3}$ electrode at 25 and 40°C. Frequency range: 10 kHz to 0.001 Hz. The real part was corrected for the ohmic resistance between the working and the reference electrode. Measurements were made at open-circuit potential. The inset in the bottom panel is a plot for the full frequency range at 40°C after the electrode was discharged for 82 min. It shows the rapid increase in the imaginary part of the impedance at low frequencies.

Downloaded on 2017-02-26 to IP 129.10.247.223 address. Redistribution subject to ECS terms of use (see ecsdl.org/site/terms_use) unless CC License in place (see abstract).

S0013-4651(99)01-045-9 CCC: $7.00 © The Electrochemical Society, Inc.

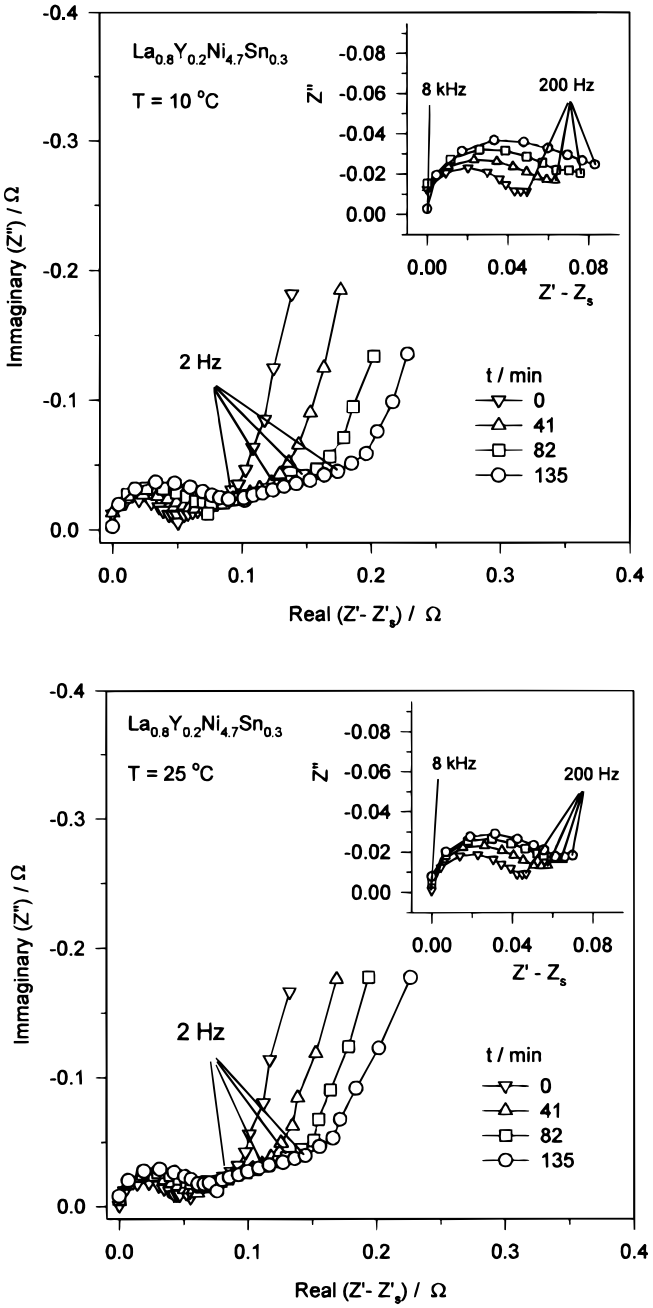

Figure 6. Nyquist plots expanded in the high-frequency domain at several SOC for a $La_{0.8}Y_{0.2}Ni_{4.7}Sn_{0.3}$ electrode at 10 and 25°C. Representative frequency values are indicated in the figures. Real part was corrected for the ohmic resistance between the working and the reference electrode. Measurements were made at open-circuit potential.

2. Features in the range of ca. 200 to ca. 2 Hz.—From the results of Fig. 6 and 7b it is clear that this feature appears as a linear region, the extent of which is dependent on the SOC and on the temperature. It is most likely related to the diffusion processes taking place inside the MH particles, as proposed by Wang.[28] However, the assignment by Zhang *et al.*[21] to particle-to-particle electronic conductance of the MH electrodes is also plausible.

3. Arc in the range of 2 Hz to 10 mHz.—The magnitude and the characteristic frequency of this feature are dependent on the alloy composition, the state of charge, and the temperature (Fig. 4 and 5). In accordance with what has been proposed for most metal hydrides,[20-27] this feature is associated with the charge-transfer step at the electrode/electrolyte interface. It is noted that the decrease of resistance with decreasing SOC is accompanied by an increase in the characteristic frequency, which is in accordance with EIS principles. Also, from the results of Fig. 7 it is observed that the values of the resistance exhibit an exponential decrease with increase in temperature, which is the expected behavior for the charge-transfer resistance.

4. Features at frequencies < 10 mHz.—At frequencies < 10 mHz, for $T \leq 25$°C and for SOC $\geq 50\%$, no further features are seen in fully charged electrodes. However, at lower SOC, particularly at high temperatures, the imaginary component of the impedance undergoes a moderate increase, which is followed by a steep increase at lower frequencies. This is illustrated in the inset in the bottom of Fig. 5.

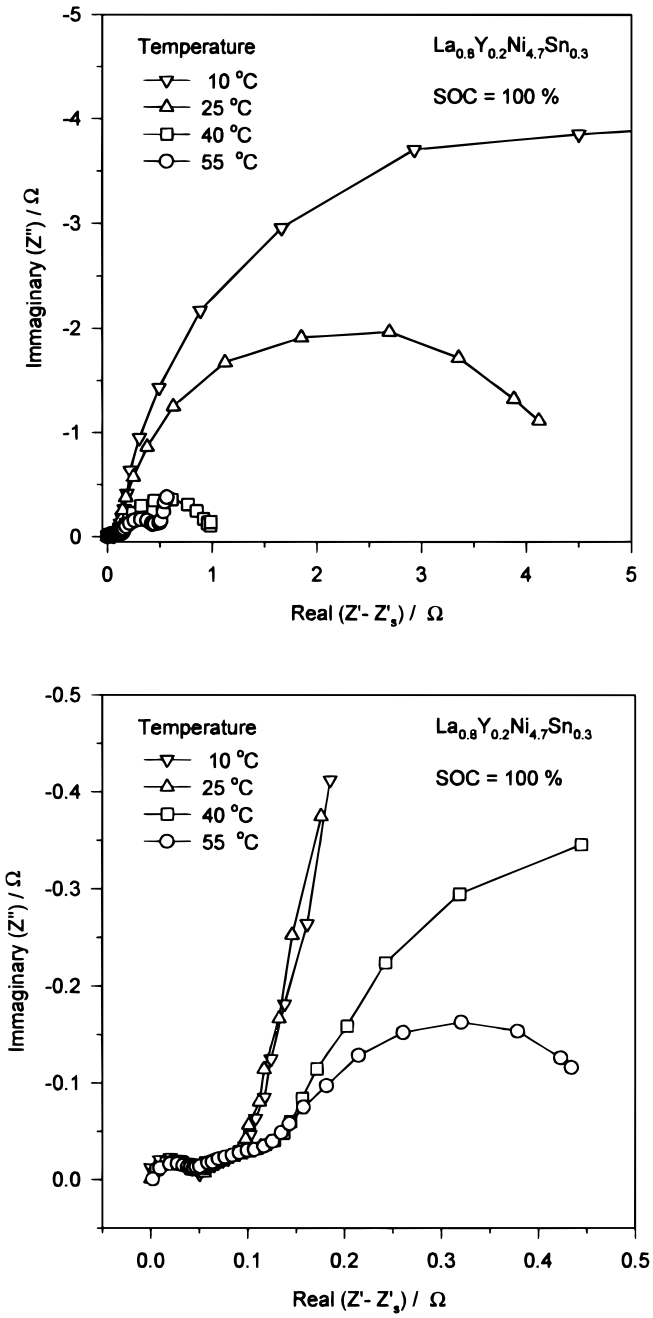

Figure 7. (Top) Nyquist plots at 100% SOC for a $La_{0.8}Y_{0.2}Ni_{4.7}Sn_{0.3}$ electrode as a function of temperature. Frequency range: 10 kHz to 0.001 Hz . Real part was corrected for the ohmic resistance between the working and the reference electrode. Measurements were made at open-circuit potential. (Bottom) Same results expanded in the high-frequency domain.

Downloaded on 2017-02-26 to IP 129.10.247.223 address. Redistribution subject to ECS terms of use (see ecsdl.org/site/terms_use) unless CC License in place (see abstract).

S0013-4651(99)01-045-9 CCC: $7.00 © The Electrochemical Society, Inc.

Table III. Summary of kinetic from EIS at various SOC.

SOC	$LaNi_{4.7}Sn_{0.3}$-activated (eight cycles)		$La_{0.8}Y_{0.2}Ni_{4.7}Sn_{0.3}$-activated (20 cycles)	
%	j_o at 25°C (mA g^{-1})	E_a (kJ mol^{-1})	j_o at 25°C (mA g^{-1})	E_a (kJ mol^{-1})
100	87	32	58	39
75	88	36	79	38
50	97	36	116	39
23	98	—	155	—

This was observed for both alloys. This feature has been assigned to the capacitive behavior of a fully discharged alloy.[24,26,27]

The charge-transfer resistance (R_{ct}) at the electrode/electrolyte interface is given by (η/j), and the ac measurements were made for $\eta \approx 0$, so that Eq. 5 can also be used to obtain the exchange current density of the HOR from R_{ct} data. Table III presents these values for the activated $LaNi_{4.7}Sn_{0.3}$ and $La_{0.8}Y_{0.2}Ni_{4.7}Sn_{0.3}$ alloys at several SOC at 25°C. The kinetic data obtained from impedance measurements (Table III) are consistent with those obtained from the galvanodynamic experiments (Table II). The values of the exchange current density and the activation energies of the HOR, obtained by both methods, for $LaNi_{4.7}Sn_{0.3}$ and $La_{0.8}Y_{0.2}Ni_{4.7}Sn_{0.3}$ at SOC 100% are very similar (Tables II and III). Also, Table II shows that, even though a small difference in the values of E_a is present, the values j_o for the hydrogen evolution reaction (HER) obtained for fully charged electrodes are very close to those of the HOR, as would be expected from the principles of microscopic reversibility. Since for a fully charged electrode no diffusion components inside the alloy are expected, this provides further evidence for the assignment of the impedance feature discussed in item 3 above to the charge-transfer resistance of the HOR.

Table II shows that the presence of Y, in any amount, decreases the exchange current density (j_o) for the charge/discharge processes. However, within experimental error, the activation energies are essentially the same in the presence or absence of Y. From these results it is concluded that the differences in the charge/discharge reaction kinetics are merely a consequence of the different surface area of the alloys. When the electrodes with $x = 0$ and $x = 0.2$ were cycled 130 times, there was an increase of j_o, an effect that is associated with the increase of surface area with cycling.

Table III shows that the exchange current density for $La_{0.8}Y_{0.2}Ni_{4.7}Sn_{0.3}$ increases with decreasing state of charge, while the activation energy remains relatively constant. In the case of $LaNi_{4.7}Sn_{0.3}$ the increase in j_o with depth of discharge was much less. This behavior of j_o is consistent with the results of Fig. 1, where the increase in the electrode potential as a function of discharge time was much more obvious for the sample with Y. An increase of j_o with the decrease of SOC has been also reported for several other metal hydrides.[20,22,25,27] In alkaline water electrolyzers, it is well known that the exchange current density of hydrogen evolution on the nickel cathodes decreases with time. This has been attributed to hydriding of the nickel.[33] A similar mechanism may be occurring here on the metallic surface species responsible for the catalytic surface processes. Dehydriding of these species, with decreasing SOC, increases the exchange current density of the HOR. Another possibility is that the discharged material contains two phases, with one only active for the HOR. Decreasing SOC could increase the proportion of the active phase, resulting in an increase in j_o while keeping E_a constant. Another possibility is catalysis by an increase in the amount of some oxidized species on the alloy surface with SOC.

XAS studies.—Figures 8 and 9 present representative XANES results in the transmission and electron-yield modes at the Ni K edge for uncycled metal hydride alloys. From the results in the transmission mode (Fig. 8) it is seen that, compared with Ni, the shoulder centered at 0.0 eV is higher for the metal hydride alloys, and the edge position is shifted by *ca*. 2.0 eV below that found for Ni. No apparent effect is introduced by replacement of La by Y or of Ni by Co. In the case of the electron-yield mode (Fig. 9), the edge shift is somewhat smaller than in the transmission mode, and the pre-edge shoulder centered at 0.0 eV has essentially the same magnitude as for pure Ni.

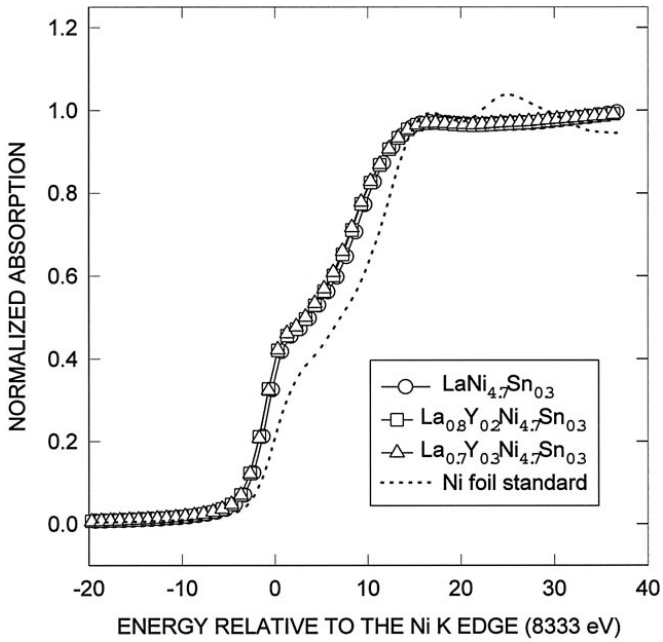

Figure 8. XANES spectra in the transmission mode, at the Ni K edge, for uncycled gas-activated $La_{(1-x)}Y_xNi_{4.7}Sn_{0.3}$ electrodes ($x = 0$, 0.2, and 0.3), and for a Ni foil.

The main absorption feature at the Ni K edge is due to the excitation of 1s electrons into empty 4p states, which is dipole allowed. The prewave at 0.0 eV is attributed to weak quadrupole-allowed transitions for systems with cubic or octahedral symmetry (*e.g.*, pure Ni). In the case of the metal hydride alloys, the symmetry is hexagonal;

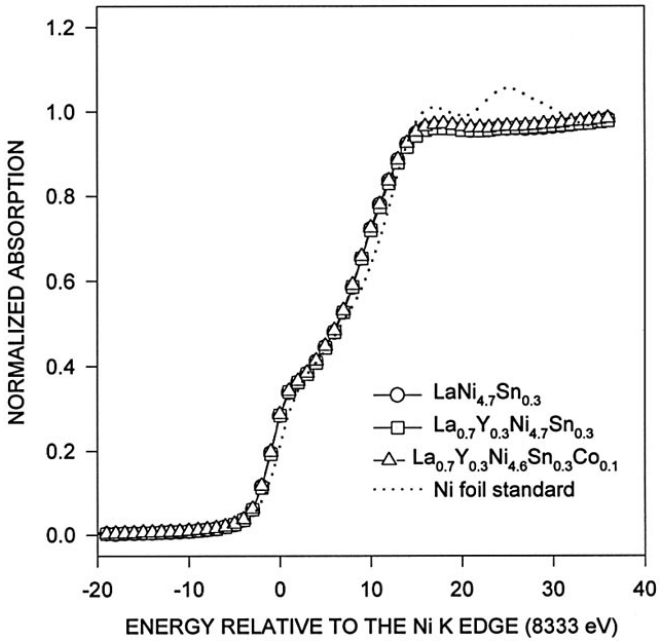

Figure 9. XANES spectra in the electron-yield mode at the Ni K edge for uncycled gas-activated $LaNi_{4.7}Sn_{0.3}$, $La_{0.7}Y_{0.3}Ni_{4.7}Sn_{0.3}$, and $La_{0.7}Y_{0.3}Ni_{4.6}Sn_{0.3}Co_{0.1}$. Transmission data for a Ni foil are also shown.

Downloaded on 2017-02-26 to IP 129.10.247.223 address. Redistribution subject to ECS terms of use (see ecsdl.org/site/terms_use) unless CC License in place (see abstract).

S0013-4651(99)01-045-9 CCC: $7.00 © The Electrochemical Society, Inc.

thus there is a mixing of Ni p and d states, and electronic transitions into empty states of primarily d character may also occur. This leads to a higher intensity of the peak at 0.0 eV. This can be taken as an indirect measure of the density of empty d states above the Fermi level.[9]

The data obtained in the transmission mode give information on bulk properties, whereas those for the electron yield are more surface sensitive. In the transmission mode the intensity of the pre-edge shoulder is higher than in the electron-yield mode, and thus the properties of the Ni atoms in the bulk of the alloy particles must be somewhat different from those on the surface, with the latter having a smaller overlap of p-d orbitals and/or a smaller number of empty d states. The Ni XANES is the same in the presence or absence of Y (for both transmission and electron-yield modes), indicating that the electronic structure of the alloy is minimally affected when La is replaced by Y. This is why the HOR kinetics is not affected by the presence of Y, as seen in Table II.

Figures 10 and 11 compare the XANES spectra obtained at the Ni K edge in the transmission and electron-yield modes, respectively, for uncycled and cycled (100 times) dehydrided electrodes. Figure 12 presents the results obtained in the electron-yield mode, after 300 cycles. The spectra in the transmission mode (Fig. 10) for the uncycled and cycled electrodes are similar, except for a small reduction in the magnitude of the pre-edge shoulder for the cycled samples, especially for the alloy without Y. Besides the pre-edge effect, spectra in the electron-yield mode for the cycled samples (Fig. 11 for 100 cycles and Fig. 12 for 300 cycles) have an enhanced white line which is absent in the uncycled samples. Comparison of results of Fig. 11 and 12 clearly shows that there is an increase in the white line magnitude with cycling. Since the corrosion product is accumulated on the particle surface, its presence is more apparent from measurements in the electron-yield spectra, as clearly confirmed by comparison of the results in Fig. 10 and 11. There is a clear reduction in the white line (Fig. 11 and 12) as the Y content is increased, indicating reduction in Ni corrosion introduced by Y. This is the reason for the improved lifetime of the Y containing metal hydride alloys.

Figure 13 compares XANES spectra obtained at the Y K edge (transmission mode) for uncycled and activated/charged $La_{0.7}Y_{0.3}Ni_{4.7}Sn_{0.3}$. The spectrum of the charged alloy was obtained *in situ* according to a procedure described elsewhere.[9] Comparison of spectra in Fig. 13 shows that, except for a small positive shift of the edge position, activation and charging the alloy introduce only very small changes in the electronic structure of Y. The edge shift to higher energies on hydriding indicates that some tetrahedral sites associated with Y atoms also participate in the hydriding reactions.

Figure 14 presents XANES spectra, at the Y K edge, for uncycled and cycled (100 times) $La_{0.7}Y_{0.3}Ni_{4.7}Sn_{0.3}$. As in the case of Ni, the XANES at the Y K edge for uncycled and activated samples were similar (not shown); also, the results for samples cycled up to 300 times (not shown) were essentially the same as that for 100 cycles. The spectrum of Y in the uncycled alloy is similar to that of the bulk

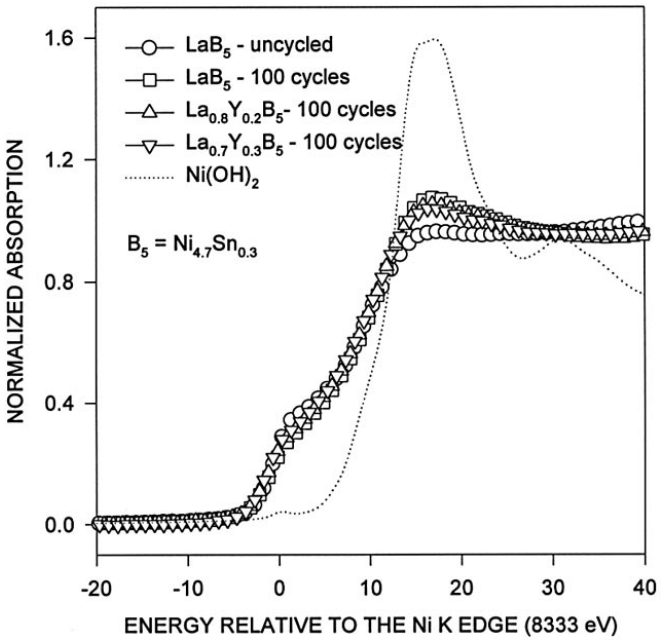

Figure 11. XANES spectra in the electron-yield mode at the Ni K edge for uncycled LaB_5 ($B_5 = Ni_{4.7}Sn_{0.3}$) and cycled (100 cycles) LaB_5, $La_{0.8}Y_{0.2}B_5$, and $La_{0.7}Y_{0.3}B_5$. Data for $Ni(OH)_2$ in the transmission mode are also shown.

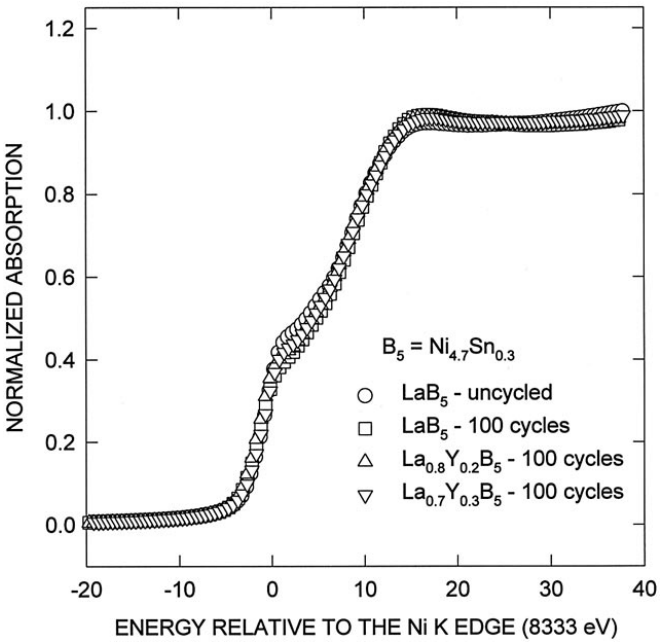

Figure 10. XANES spectra in the transmission mode at the Ni K edge for uncycled gas-activated LaB_5 ($B_5 = Ni_{4.7}Sn_{0.3}$) and cycled (100 cycles) LaB_5, $La_{0.8}Y_{0.2}B_5$, and $La_{0.7}Y_{0.3}B_5$.

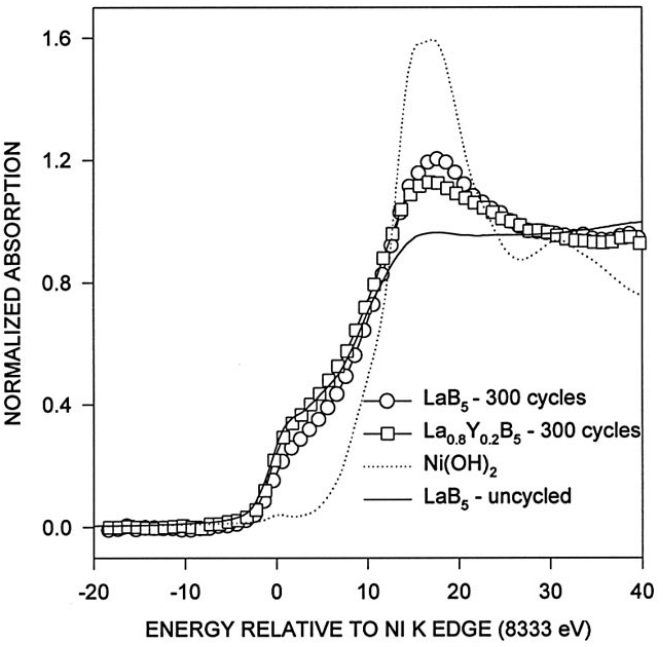

Figure 12. XANES spectra in the electron-yield mode at the Ni K edge for uncycled gas-activated LaB_5 ($B_5 = Ni_{4.7}Sn_{0.3}$) and cycled (300 cycles) LaB_5 and $La_{0.8}Y_{0.2}B_5$. Data for $Ni(OH)_2$ in the transmission mode are also shown for comparison.

Downloaded on 2017-02-26 to IP 129.10.247.223 address. Redistribution subject to ECS terms of use (see ecsdl.org/site/terms_use) unless CC License in place (see abstract).

S0013-4651(99)01-045-9 CCC: $7.00 © The Electrochemical Society, Inc.

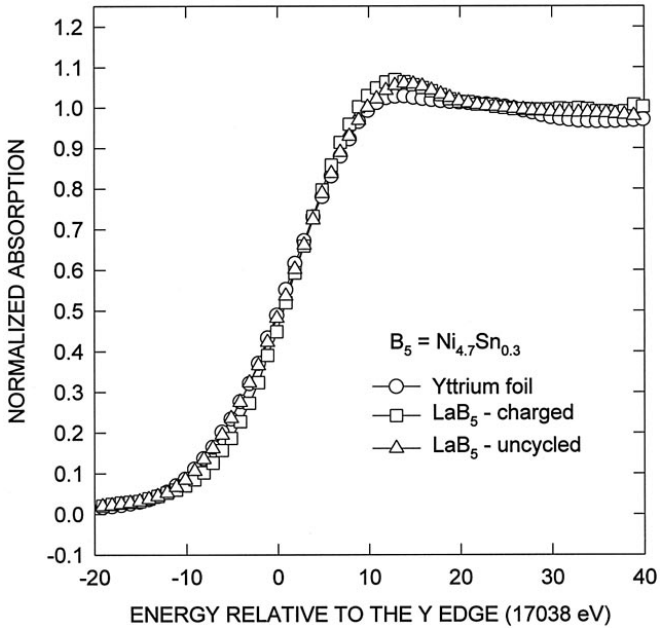

Figure 13. XANES spectra in the transmission mode at the Y K edge for Y foil and uncycled gas-activated $La_{0.7}Y_{0.3}B_5$. Also shown are *in situ* Y XANES for charged $La_{0.7}Y_{0.3}B_5$. Measurements in the charged state were made *in situ*,[9] after electrochemical activation of the alloy.

metal (Fig. 13 and 14). The samples cycled 100 times show an enhanced white line that is approximately the same as for a sample cycled 300 times. As in the case of Ni, this behavior can be attributed to the formation of Y hydrous oxides upon cycling. However, as opposed to Ni, the amount of Y hydrous oxides remains essentially constant after *ca*. 100 cycles, which is consistent with formation of a finite surface layer of the product with no further buildup beyond 100 cycles.

The alloys with Y have a lower exchange current or equivalently a smaller surface area than in the absence of Y. Table II shows that

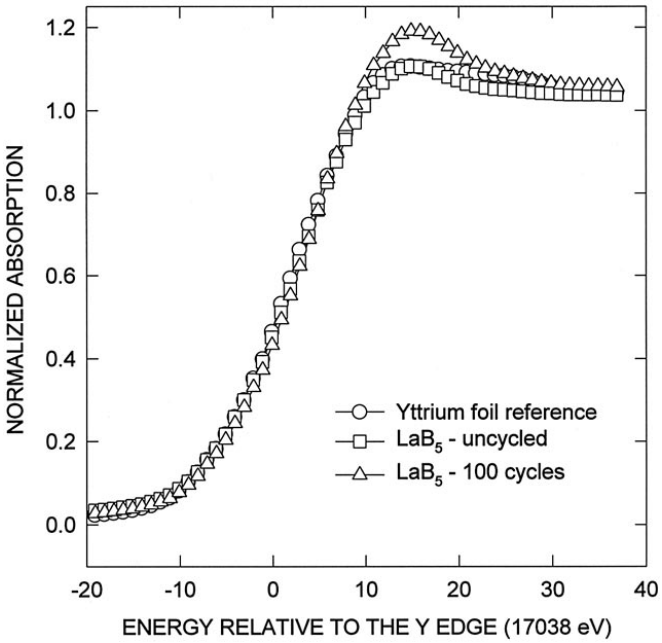

Figure 14. XANES spectra in the transmission mode at the Y K edge for Y foil, uncycled gas-activated $La_{0.7}Y_{0.3}B_5$ and $La_{0.7}Y_{0.3}B_5$ after cycling for 100 cycles.

the ratio of increase of the exchange current density (Table II) with cycling is similar for the samples with and without Y, indicating a proportional enlargement of the alloy surface area as cycling progresses. Therefore, the protection of Y cannot be ascribed to less pulverization of the alloy on cycling. Also, the rate of capacity decay in Table I shows no direct relationship to the exchange current density, and therefore no relationship with the alloy surface area, indicating that the protecting mechanism is not related to the surface area or the particle size. It must be concluded then that the corrosion-protection mechanism is associated with the presence of a physical barrier of Y hydrous oxide, which acts as a blocking passivating layer.

Conclusions

Partial substitution of La by Y greatly improves the cycling stability of $LaNi_{4.7}Sn_{0.3}$-type metal hydride, with the best results found for $La_{0.8}Y_{0.2}Ni_{4.7}Sn_{0.3}$. There is a small reduction in the initial electrode discharge capacity (*ca*. 10%) in $La_{0.8}Y_{0.2}Ni_{4.7}Sn_{0.3}$, but after 300 cycles, the respective capacities for $LaNi_{4.7}Sn_{0.3}$ and $La_{0.8}Y_{0.2}Ni_{4.7}Sn_{0.3}$ were 100 and 200 mAh g^{-1}. The reaction kinetics is slower for the Y substituted alloys, but the differences are merely consequences of the differences in the surface areas of the alloys.

Electrode-kinetic studies using steady-state methods as well as galvanodynamic and EIS techniques yielded consistent results. EIS studies at various temperatures greatly aided the interpretation of the EIS spectra. The exchange current density of the HOR on the Y containing alloys shows a marked increase with increasing depth of discharge. This has been attributed to dehydriding of the metallic catalytic species on the surface of the MH particles as discharge progresses.

XANES results clearly indicate a reduction of Ni corrosion in the alloys with Y. This is the main reason for improvement of the cycle life. However, the diminution of Ni corrosion promoted by Y is not associated with any change in the electronic structure of the alloy or to reduced pulverization of the alloy. It is proposed that the corrosion-protection mechanism must be associated with the presence of a physical barrier of a Y hydrous oxide acting as a blocking passivating layer.

Acknowledgments

The authors acknowledge the support of the U.S. Department of Energy under contract no. DA-AC02-98CH10886. E.A.T. is on leave of absence from Instituto de Química de São Carlos/USP, Brazil, with a scholarship from Fundação de Amparo a Pesquisa do Estado de São Paulo (FAPESP).

Brookhaven National Laboratory assisted in meeting the publication costs of this article.

References

1. B. V. Ratnakumar, C. Witham, R. C. Bowman, Jr., A. Hightower, and B. Fultz, *J. Electrochem. Soc.*, **143**, 2578 (1996), and references cited therein.
2. G. D. Adzic, J. R. Johnson, S. Mukerjee, J. McBreen, and J. J. Reilly, *J. Alloys Comp.*, **253-254**, 579 (1997).
3. B. V. Ratnakumar, G. Halpert, C. Witham, and B. Fultz, *J. Electrochem. Soc.*, **141**, 189 (1994).
4. B. V. Ratnakumar, S. Surampudi, S. Di Stefano, G. Halpert, C. Witham, A. Hightower, and B. Fultz, in *Hydrogen and Metal Hydride Batteries*, P. D. Bennett and T. Sakai, Editors, PV 94-27, p. 57, The Electrochemical Society Proceedings Series, Pennington, NJ (1994).
5. C. Witham, R. C. Browman, Jr., B. V. Ratnakumar, B. Fultz, and S. Surampudi, *Proc. IEEE*, 129 (1996).
6. C. Witham, B. V. Ratnakumar, R. C. Bowman, Jr., A. Hightower, and B. Fultz, *J. Electrochem. Soc.*, **143**, L206 (1996).
7. G. D. Adzic, J. R. Johnson, J. J. Reilly, J. McBreen, S. Mukerjee, M. P. S. Kumar, W. Zang, and S. Srinivasan, *J. Electrochem. Soc.*, **142**, 3429 (1995).
8. M. E. Fiorino, R. L. Opila, K. Konstadinidas, and W. C. Fang, *J. Electrochem. Soc.*, **143**, 2422 (1996).
9. S. Mukerjee, J. McBreen, J. J. Reilly, J. R. Johnson, G. Adzic, K. Petrov, M. P. S. Kumar, W. Zang, and S. Srinivasan, *J. Electrochem. Soc.*, **142**, 2278 (1995).
10. S. Mukerjee, J. McBreen, J. J. Reilly, J. R. Johnson, G. D. Adzic, and M. R. Marrero, Absract 290, p. 353, The Electrochemical Society and International Society of Electrochemistry Meeting Absracts, Vol. 97-2, Paris, France, Aug 31-Sept 5, 1997.
11. S. Srinivasan, W. Zang, M. P. S. Kumar, A. Visintin, S. Mukerjee, J. McBreen, G. Adzic, J. R. Johnson, J. J. Reilly, R. B. Schwarz, M. L. Wasz, and H. S. Lim, in *Electrode Materials and Processes for Energy Conversion and Storage IV*, J. McBreen, S. Mukerjee, and S. Srinivasan, Editors, PV 97-13, p. 265, The Elec-

Downloaded on 2017-02-26 to IP 129.10.247.223 address. Redistribution subject to ECS terms of use (see ecsdl.org/site/terms_use) unless CC License in place (see abstract).

S0013-4651(99)01-045-9 CCC: $7.00 © The Electrochemical Society, Inc.

trochemical Society Proceedings Series, Pennington, NJ (1997).
12. A. Zuttel, F. Meli, and L. Schlapbach, *J. Alloys Comp.*, **221**, 207 (1995).
13. Q. M. Yang, M. Ciureanu, D. H. Ryan, and J. O. Strom-Olsen, *J. Electrochem. Soc.*, **141**, 2108 (1994).
14. Q. M. Yang, M. Ciureanu, D. H. Ryan, and J. O. Strom-Olsen, *J. Electrochem. Soc.*, **141**, 2113 (1994).
15. G. Zheng, B. N. Popov, and R. E. White, *J. Electrochem. Soc.*, **142**, 2695 (1995).
16. Y. Fukumoto, M. Miyamoto, M. Matsuoka, and C. Iwakura, *Electrochim. Acta*, **40**, 845 (1995).
17. C. Iwakura, M. Miyamoto, H. Inoue, M. Matsuoka, and Y. Fukumoto, *J. Alloys Comp.*, **231**, 558 (1995).
18. C. Iwakura, M. Miyamoto, H. Inoue, M. Matsuoka, and Y. Fukumoto, *J. Electroanal. Chem.*, **411**, 109 (1996).
19. H. Inoue, M. Miyamoto, M. Matsuoka, Y. Fukumoto, and C. Iwakura, *Electrochim. Acta*, **42**, 1087 (1997).
20. H. Yang, Y. Zhang, Z. Zhou, J. Wei, G. Wang, D. Song, X. Cao, and C. Wang, *J. Alloys Comp.*, **231**, 625 (1995).
21. W. Zhang, M. P. Kumar, S. Srinivasan, and H. J. Ploehn, *J. Electrochem. Soc.*, **142**, 2936 (1995).
22. G. Zheng, B. N. Popov, and R. E. White, *J. Electrochem. Soc.*, **143**, 435 (1996).
23. N. Cui, B. Luan, H. J. Zhao, H. K. Liu, and S. X. Dou, *J. Alloys Comp.*, **248**, 159 (1997).
24. B. Reichman, W. Mays, M. A. Fetcenko, and S. R. Ovshinsky, in *Electrochemical Surface Science of Hydrogen Adsorption and Absorption*, G. Jerkiewicz and P. Marcus, Editors, PV 97-16, p. 236, The Electrochemical Society Proceedings Series, Pennington, NJ (1997).
25. L. O. Valoen, S. Sunde, and R. Tunold, *J. Alloys Comp.*, **253-254**, 656 (1997).
26. P. Millet and P. Dantzer, *J. Alloys Comp.*, **253-254**, 542 (1997).
27. W-K. Hu, H. Lee, D-M. Kim, S-W. Jeon, and J-Y. Lee, *J. Alloys Comp.*, **268**, 261 (1998).
28. C. Wang, *J. Electrochem. Soc.*, **145**, 1801 (1998).
29. W. T. Elam, J. P. Kirkland, R. A. Neiler, and P. E. Wolf, *Phys. Rev. B.*, **38**, 26 (1988).
30. D. E. Sayers and D. A. Bunker, in *X-Ray Absorption: Principles, Applications, Techniques of EXAFS, SEXAFS, and XANES*, D. C. Koningsberger and R. Prins, Editors, John Wiley & Sons, Inc., New York (1988).
31. S. Mukerjee, S. Srinivasan, M. P. Soriaga, and J. McBreen, *J. Electrochem. Soc.*, **142**, 1409 (1995).
32. S. Mukerjee, S. Srinivasan, M. P. Soriaga, and J. McBreen, *J. Phys. Chem.*, **99**, 4577 (1995).
33. H. E. G. Rommal and P. J. Moran, *J. Electrochem. Soc.*, **135**, 343 (1988).

Downloaded on 2017-02-26 to IP 129.10.247.223 address. Redistribution subject to ECS terms of use (see ecsdl.org/site/terms_use) unless CC License in place (see abstract).